Quantum-enhanced microscopic imaging technology [Invited]

Jun Liu (刘 军)[1] and Xiaolong Su (苏晓龙)[1,2*]

[1] State Key Laboratory of Quantum Optics and Quantum Optics Devices, Institute of Opto-Electronics, Shanxi University, Taiyuan 030006, China

[2] Collaborative Innovation Center of Extreme Optics, Shanxi University, Taiyuan 030006, China

*Corresponding author: suxl@sxu.edu.cn

Microscopes are indispensable tools in modern biology and medicine. With the development of microscopy, the signal-to-noise ratio of microscopes is now limited by the shot noise. Recently, quantum-enhanced microscopic imaging provides a feasible approach for improving the signal-to-noise ratio since it can beat the shot-noise limit by using quantum light. In this review, we first briefly introduce quantum states applied in quantum-enhanced microscopic imaging, and then we provide an overview of the principle and progress of quantum-enhanced stimulated Raman scattering microscopy, entangled two-photon microscopy, and quantum-enhanced differential interference contrast microscopy.

Keywords: squeezed state; entangled state; imaging; microscopy.
DOI: 10.3788/COL202422.060010

1. Introduction

The invention of microscopes opened the door to explore the microscopic world and brought about groundbreaking revolution to the development of biology and medicine[1]. Since the first microscope was applied in microbiology[2], various types of microscopes have been successively developed. For example, the transmission electron microscope significantly improved the resolution of the microscope to the nanometer level by replacing the light with an electron beam[3]. Furthermore, the fluorescence microscope is widely used to study the distribution and transport of substances within cells, thanks to its high contrast and intrinsic selectivity[4]. Combined with laser scanning confocal microscopy[5], the fluorescence microscope has become one of the most commonly used devices in modern biological and medical experiments. Benefiting from the development of microscopic technology, significant advances have been made in the fields of biology and medicine.

There are several parameters that are used to evaluate the performance of the microscope, for instance, the sensitivity and resolution. The sensitivity of the microscope is related to the signal-to-noise ratio (SNR) of the image. To further improve the sensitivity in the case of avoiding damage of the sample with a high power signal, it is necessary to reduce the noise background, which is limited by shot noise. As the minimum noise level in the classical world, the shot noise cannot be reduced with classical technologies. Thus, it is important to employ quantum technologies to beat shot noise, which leads to the enhancement of the SNR and the improvement of the sensitivity.

Quantum technologies have been widely applied in the fields of quantum information, including quantum communication[6–10], quantum computation[11–14], and quantum metrology[15–19]. Moreover, several quantum imaging technologies have been developed[20,21]. For example, ghost imaging with entangled photon pairs is capable of imaging an object by correlating the output of a bucket detector, which collects light that has been transmitted through or reflected from an object, and the multi-pixel detector whose illumination has not interacted with that object[22–27]. Another fascinating imaging technique is quantum illumination[28–33], which can detect and image objects even with high losses and background noise by exploiting quantum states of light. In addition to these quantum imaging techniques, quantum-enhanced microscopic imaging technologies are also developed to reduce the probe power[34] and improve the SNR of imaging[35–38]. Compared with conventional microscopy, the enhancement of quantum-enhanced microscopic imaging comes from the use of quantum light, such as squeezed light, entangled photon pairs, and NOON state.

In this review, we mainly focus on a brief review of quantum-enhanced microscopy with different quantum states of light. In Section 2, we briefly introduce the basic characteristics and preparation methods of several typical quantum states. Then, in Sections 3, 4, and 5, respectively, we overview the principle and progress of stimulated Raman scattering (SRS) microscopy based on the squeezed state, two-photon absorption (TPA) fluorescence microscopy based on entangled photon pairs, and differential interference contrast microscopy (DIM) based on the NOON state. Lastly, we briefly summarize the review and

discuss the challenges of quantum-enhanced microscopic imaging in the future.

2. Quantum Light Source Used in Quantum-Enhanced Microscopic Imaging

2.1. Squeezed light

The minimum noise level that can be reached in the classical regime is the noise of the vacuum state and/or coherent state, which corresponds to the shot-noise limit (SNL). For a quantum state of light, the variances of the amplitude quadrature $\Delta^2 \hat{X}$ and the phase quadrature $\Delta^2 \hat{P}$ of it are restricted by Heisenberg's uncertainty principle,

$$\Delta^2 \hat{X} \cdot \Delta^2 \hat{P} \geq 1, \tag{1}$$

where $\hat{X}$ and $\hat{P}$ are defined by the annihilation $\hat{a}$ and generation $\hat{a}^\dagger$ operators, with the following expression:

$$\hat{X} = \hat{a} + \hat{a}^\dagger, \quad \hat{P} = -i(\hat{a} - \hat{a}^\dagger), \tag{2}$$

respectively.

The Wigner function of the vacuum state, the coherent state, the amplitude squeezed state, and the phase squeezed state are shown in Figs. 1(a)–1(d), respectively[39]. The variances of the quadratures of the vacuum state and coherent state are $\Delta^2 \hat{X} = \Delta^2 \hat{P} = 1$, which corresponds to the SNL. It is obvious that the noise of one quadrature of squeezed light can be lower than the SNL at the expense of increased noise variance in the conjugated quadrature, which makes it possible to improve the SNR in microscopic imaging.

Usually, the squeezed state can be prepared by the progress of parametric down-conversion based on second-order nonlinear optical effects. For femtosecond or picosecond pulses, strong nonlinear effects appear when it passes through a nonlinear crystal just one time, as its extremely high peak power[40]. A pulsed squeezed light with a squeezing level of −5.0 dB has been experimentally prepared[41]. For continuous waves, nonlinear interactions can be enhanced through the use of a resonant cavity, as shown in Fig. 1(e)[42]. The continuous-wave single-mode squeezed light with a squeezing level of up to −15 dB has been experimentally demonstrated[43]. In addition to the parametric down-conversion in a nonlinear crystal, the four-wave mixing process in the atomic assemble is the other method for preparing squeezed light, as shown in Fig. 1(g)[44]. By using two tuned strong pumps ν_1 and ν_2, the squeezed vacuum and the quadrature-squeezed bright beam can be prepared with the presence and absence of weak probe ν_p, respectively. In addition, other methods for generating squeezed states have also been developed, including photonic crystal fibers[45] and integrated optical quantum chips[46,47], which enhance the scalability of the quantum light source.
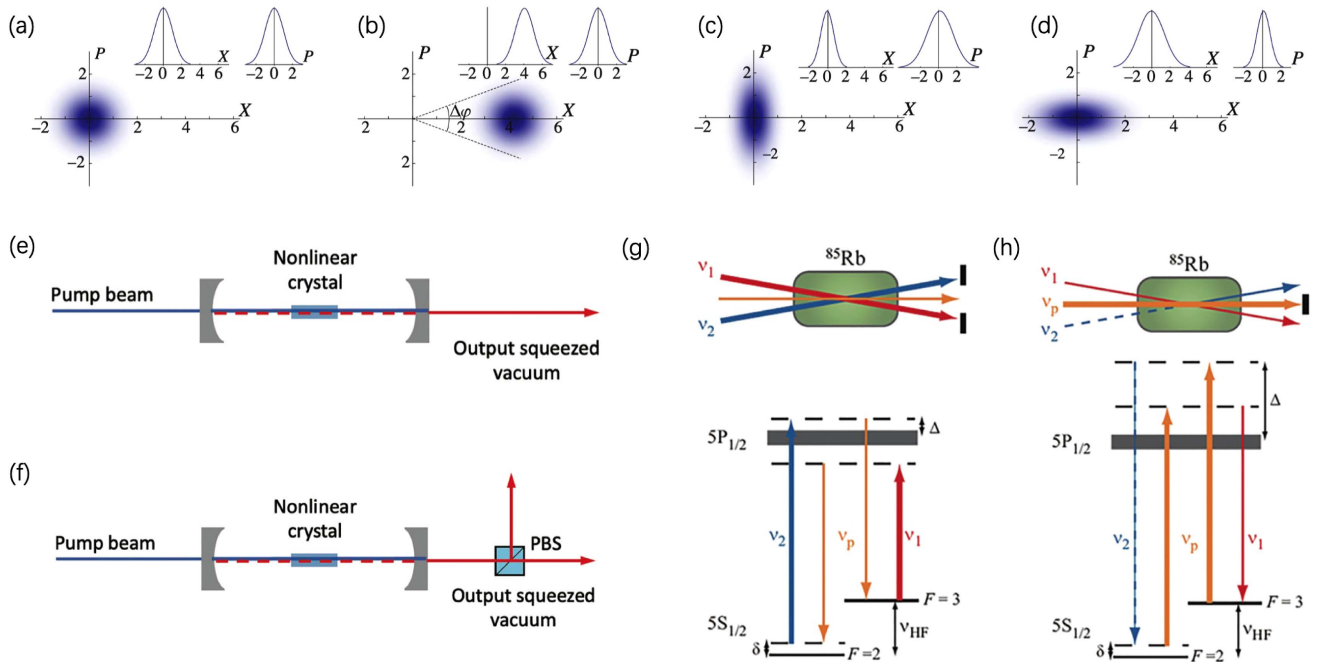

Fig. 1. Characteristics and preparation methods of the squeezed states and the entangled states. (a)–(d) Wigner functions of (a) the vacuum state, (b) the coherent state, (c) the quadrature amplitude squeezed vacuum state, and (d) the quadrature phase squeezed vacuum state. Insets show the edge distribution of Wigner function[39]. (e) Parametric down-conversion based on degenerate optical parametric amplifier. (f) Parametric down-conversion based on non-degenerate optical parametric amplifier[42]. (g), (h) Single-mode and two-mode squeezed state generated from the four-wave mixing process in the atomic ensemble[44].

2.2. Entangled state

The entangled state is an important quantum resource. According to the quantum variables involved, there are two kinds of entangled states: the continuous-variable and the discrete-variable entangled states. For a two-mode continuous-variable entangled state, the noises of the correlated amplitude (phase) quadratures and anticorrelated phase (amplitude) quadratures are all below the corresponding SNL, which are expressed by

$$\Delta^2(\hat{X}_1 - \hat{X}_2) < \text{SNL}, \quad \Delta^2(\hat{P}_1 + \hat{P}_2) < \text{SNL}, \quad (3)$$

or

$$\Delta^2(\hat{X}_1 + \hat{X}_2) < \text{SNL}, \quad \Delta^2(\hat{P}_1 - \hat{P}_2) < \text{SNL}. \quad (4)$$

In the case of infinite squeezing, these correlated variances in Eqs. (3) and (4) trend to zero. Thus, the continuous-variable entangled state can be used to increase the SNR by applying the correlated noise to beat the SNL. The two-mode continuous-variable entangled state can be prepared by a non-degenerate optical parametric amplifier [Fig. 1(f)][42] or by a four-wave mixing process in an atomic ensemble [Fig. 1(h)][44]. Moreover, it can also be prepared by coupling two single-mode squeezed states on a beam splitter[48].

The two-photon entangled pair is a typical discrete-variable entangled state. For example, the polarization entangled photon pairs $|\Phi\rangle$ can be expressed as

$$|\Phi\rangle = |H\rangle_1|V\rangle_2 + e^{i\varphi}|V\rangle_1|H\rangle_2, \quad (5)$$

where H and V represent horizontal and vertical polarization direction, respectively, and φ is the relative phase. The two-photon entangled pair can be prepared by spontaneous parametric down-conversion (SPDC) progress in a Type-II crystal. As shown in Fig. 2(a)[49], when a pump light with high frequency ω_p is injected into a nonlinear crystal, it has a certain probability to be converted into two photons at low frequencies ω_s and ω_i, which satisfy the following relationship of energy conservation and momentum conservation:

$$\omega_p = \omega_s + \omega_i, \quad \vec{k}_p = \vec{k}_s + \vec{k}_i, \quad (6)$$

where ω_p, ω_s, ω_i and $\vec{k}_p$, $\vec{k}_s$, $\vec{k}_i$ are angular frequencies and wave vectors of the pump light, signal, and idler photons, respectively.

2.3. NOON state

The NOON state, as a kind of maximally multiphoton entangled state, can be used to enhance the sensitivity of the phase measurement from the standard quantum limit $1/\sqrt{N}$ to the Heisenberg limit $1/N$[18]. The expression of the NOON state is given by

$$|\text{NOON}\rangle_{A,B} = \frac{1}{\sqrt{2}}(|N, 0\rangle_{A,B} + |0,N\rangle_{A,B}), \quad (7)$$

where A, B are two orthogonal modes, such as horizontal and vertical polarizations. The two-photon NOON state can be prepared by the Hong–Ou–Mandel effect[50,51].

As shown in Fig. 2(b), by coupling two degenerate photons generated through the SPDC process on a beam splitter, the output state forms a two-photon NOON state due to the phenomenon of two-photon interference[52]. The three-photon NOON state can also be prepared by coupling a coherent state with degenerate SPDC photon pairs on a beam splitter, as shown in Fig. 2(c)[53]. This state is obtained after the first beam splitter and then confirmed after the second beam splitter by measuring the three-photon coincidence with single photon detectors. With the similar setup of Fig. 2(c) and by manipulating the amplitude of the coherent state, it is possible to arbitrarily obtain NOON states with multiphotons[54,55].
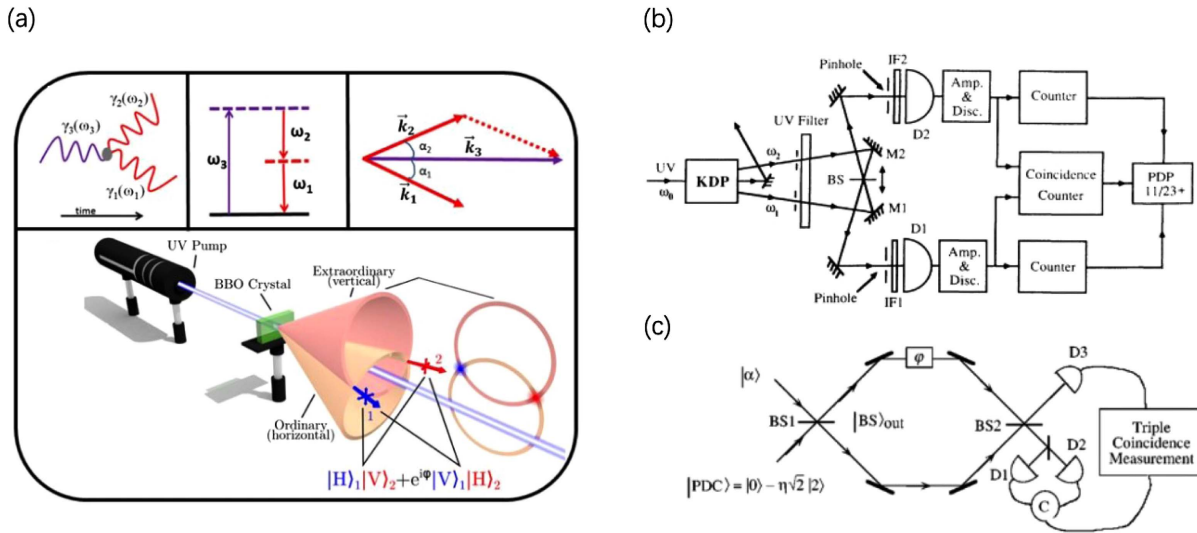
(a)

(b)

(c)

Fig. 2. (a) Preparation of entangled photon pairs[49]. (b) Preparation of the two-photon NOON state[50]. (c) Preparation of the multi-photon NOON state[53].

3. Quantum-Enhanced Stimulated Raman Scattering Microscopy

3.1. Stimulated Raman scattering microscopy

Since stimulated Raman scattering (SRS) microscopy was proposed by Xie *et al.* in 2008[56], it has been broadly applied in fields of pathological detection, biological metabolism, drug transportation, and so on[57–61]. Unlike fluorescence imaging, which normally uses fluorophores to specifically label substances[62], SRS reflects the distribution of substances or chemical bonds by detecting the vibrational or rotation modes of the molecules. This specific imaging technique eliminates the necessity for introducing external labels to the sample, thereby preventing potential damage to it. Furthermore, the SRS microscopy technology also made it easy to observe some crucial substances, such as small molecules and lipids within cells, which are difficult or unable to be fluorescently labeled[63].

As the basis of SRS microscopy, SRS is a nonlinear stimulated process that occurs when two laser beams, namely the pump beam (with frequency ω_p) and the Stokes beam (with frequency ω_s), focus on the sample simultaneously[64]. When the resonance condition $\Omega_R = \omega_p - \omega_s$ is satisfied, the stimulated Raman loss (SRL) takes place in the pump beam and the stimulated Raman gain (SRG) occurs in the Stokes beam, where Ω_R represents the vibrational frequency of the measured chemical bond. The intensities of the SRL (ΔI_p) and the SRG (ΔI_s) signals satisfy the following relationships:

$$\Delta I_p \propto -N \times \sigma_{\text{Raman}} \times I_p \times I_s,$$
$$\Delta I_s \propto N \times \sigma_{\text{Raman}} \times I_p \times I_s, \tag{8}$$

where N is the concentration of the measured chemical bonds, σ_{Raman} is the Raman scattering cross section, and I_i represents the intensity of the pump and Stokes beam, respectively. It is obvious that the SRS signal (ΔI_p or ΔI_s) is proportional to the sample concentration, which is beneficial for obtaining the distribution of the chemical bonds to be measured directly.

Although the signal intensity of the SRS has been improved for a few orders of magnitude compared to spontaneous Raman scattering, it is still quite weak compared to the intensity of the incident beam. To extract such weak signals, the phase-sensitive detection approach is often employed, as shown in Fig. 3[60]. In Fig. 3(a), one pump beam ω_p and one Stokes beam ω_s are all injected into the microscope and interact with the sample. To avoid the $1/f$ noise at low frequency and realize the shot-noise limited detection [Fig. 3(b)], the Stokes beam ω_s is applied with high-frequency intensity modulation by using an electro-optical modulator (EOM) or acousto-optical modulator (AOM). As shown in Fig. 3(c), when the SRS process happens in the sample, the modulated signal will transfer from Stokes beam ω_s to pump beam ω_p, and then the pump beam ω_p carries the SRS signal. Similarly, if we modulate the pump beam ω_p, the modulated signal transfers to Stokes beam ω_s. After passing through a filter plate, the generated SRL or SRG signal is received by a photodetector. Followed by the processes of mixing and filtering,
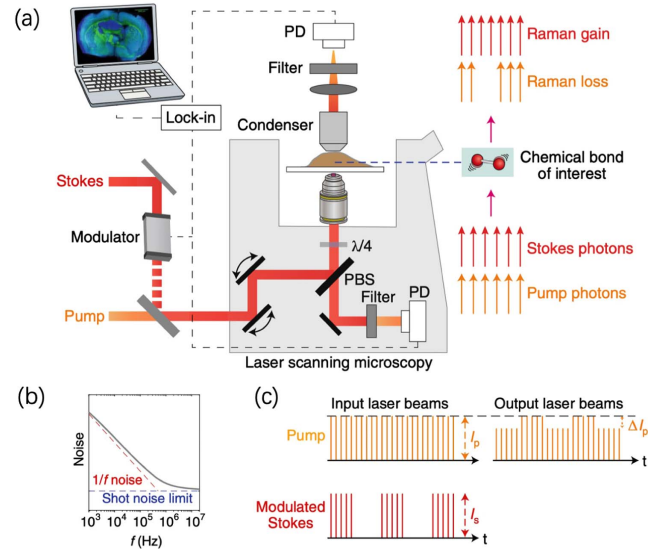

Fig. 3. (a) Setup of the SRS microscope. (b) High-frequency modulation to suppress low-frequency noise. (c) SRL signal in the pump beam[60].

the signal is demodulated through a lock-in amplifier and sent to a personal computer for further processing.

The SNR and sensitivity δN in the SRS microscopy are given by

$$\text{SNR} = \frac{KN\sigma_{\text{Raman}}I_p I_s}{\sqrt{I_s\langle X_s^2\rangle}}, \quad \delta N = \frac{\sqrt{\langle X_s^2\rangle}}{K\sigma_{\text{Raman}}I_p\sqrt{I_s}}, \tag{9}$$

where K is a constant relative to the system, and $\langle X_s^2\rangle$ represents the quadrature fluctuations of the measured signal[35]. According to Eq. (9), the SNR and sensitivity are still limited by the shot noise. Although the SNR and sensitivity can be enhanced by increasing the intensity of either the pump or Stokes beam, excessive intensity will cause damage to biological samples. Therefore, in this situation, the performance of the SRS microscope can be further improved only by reducing the noise of the probe light below the shot noise with the help of quantum light.

3.2. Quantum-enhanced stimulated Raman scattering microscopy

Compared with the coherent state, the noise of the squeezed state can be lower than the SNL. Thus, it has a potential advantage in improving the SNR of SRS microscopy. In quantum-enhanced SRS microscopy, it is essential to prepare a bright amplitude squeezed state. As shown in Fig. 4(a), by using an asymmetric (99:1) beam splitter to couple the squeezed light and coherent light, a 1.3 mW bright amplitude squeezed light with −3.6 dB squeezing has been prepared by Andrade *et al.*[35]. Another effective method used to prepare bright squeezed light is using a seeded optical parametric amplifier (OPA) directly [Fig. 4(b)]. For example, Casacio *et al.* prepared 3 mW pulsed
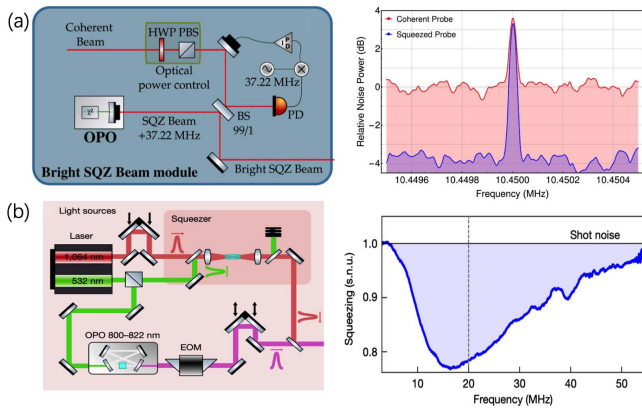
Fig. 4. Preparation of the bright squeezed light. (a) The CW bright squeezed light is prepared by coupling a squeezed vacuum state with a coherent state on a beam splitter[35]. (b) The pulsed bright squeezed light is prepared by using a seeded optical parametric amplifier[36].

bright squeezed light with -0.8 dB squeezing by using this method[36].

In quantum-enhanced SRS microscopy, the center wavelength of the squeezed light is normally fixed to reduce device complexity and enhance system stability. To realize the broad-spectrum detection of the sample, the wavelength of the other beam is tunable. By adjusting the frequency difference of the two beams to an appropriate value, the distribution of the corresponding chemical bonds can be observed. Figure 5(a) shows the SNR of polydimethylsiloxane (PDMS) at a Raman shift of 2904.76 cm^{-1} using coherent (left side) and squeezed (right side) probe beams, respectively[35]. The higher SNR observed by using squeezed light demonstrates the superiority
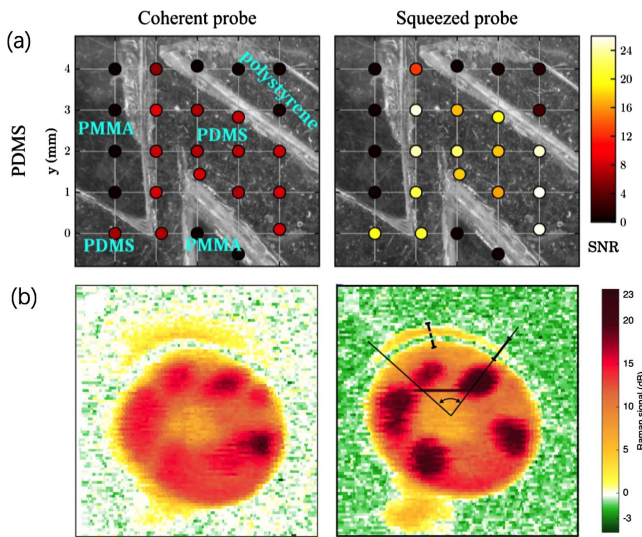
of quantum light. Figure 5(b) shows the images of a live yeast cell in an aqueous buffer at a 2850 cm^{-1} Raman shift using coherent (left side) and squeezed (right side) probe beams, respectively[36]. With the help of squeezed light, a 35% SNR improvement is achieved, which enables the observation of biological structures. This absolute quantum enhancement effectively overcomes the photodamage to live cells in SRS microscopy.

Although the quantum-enhanced SRS microscope has achieved sub-shot-noise sensitivity[36], its sensitivity has not exceeded the state-of-the-art classical SRS microscopes due to its lower power of probe (squeezed) light[37]. According to Eq. (9), the optimal SNR can be obtained when the ratio between the modulated pump light and the unmodulated probe light is 2:1[65]. For typical biological samples, their damage threshold is around several tens of milliwatts, so 3 mW of squeezed light cannot achieve the optimal SNR. To overcome this difficulty, Ozeki *et al.* proposed a quantum-enhanced balanced detection (QBD) scheme[66], which enables the detection of squeezed light with high power.

Figure 6(a) shows the schematic of SRS microscopy with the QBD scheme, where the SRL signal is measured. Different from classical SRS microscopes, in this case, pump pulses and squeezed vacuum pulses are coupled on a beam splitter. One of the output beams is directly detected by a photodetector, while the other beam is detected by another photodetector after the SRS process. By doing so, the quantum-enhanced SRS microscopy is operated in a high-power regime (> 30 mW), at the expense of 3 dB sensitivity drawback due to balanced detection[37]. Figure 6(b) shows the classical balanced-detection SRS and quantum-enhanced SRS images of d_6-DMSO and d_8-PS at a 2118 cm^{-1} Raman shift[37]. As pointed out by the red arrows, the fine structure buried in the shot noise can be found in the quantum-enhanced SRS images.
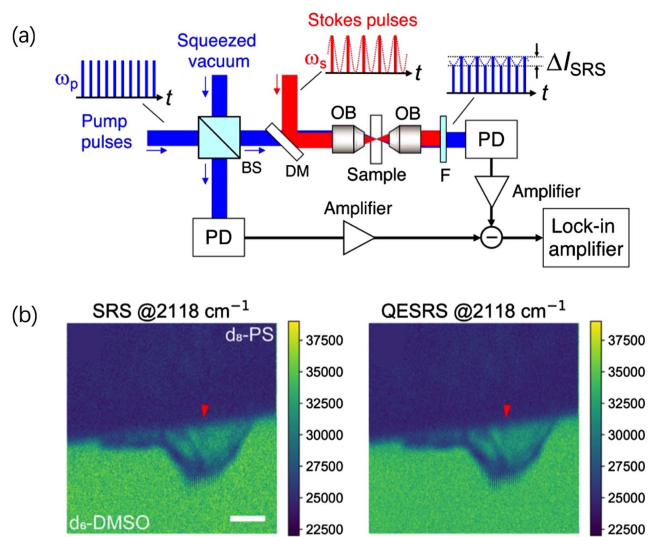

Fig. 5. (a) SNR of the polydimethylsiloxane (PDMS) at 2904.76 cm^{-1} Raman shift measured with coherent (left side) and squeezed (right side) light, respectively[35]. (b) A live yeast cell in an aqueous buffer at 2850 cm^{-1} Raman shift imaged with coherent (left side) and squeezed (right side) light, respectively[36].

Fig. 6. (a) Schematic of the SRS microscopy with QBD[66]. (b) Classical and quantum balanced-detection SRS images at Raman shift 2118 cm^{-1}. Scale bar: 10 μm[37].

4. Entangled Two-Photon Microscopy

With the help of excitation light sources such as xenon lamps or lasers, fluorescence microscopy can capture images utilizing the fluorescence emitted from the sample[4,62]. In comparison to techniques of single-photon absorption fluorescence, two-photon absorption (TPA) fluorescence microscopy employs longer-wavelength light as the excitation source. This not only enhances imaging depth but also reduces interference from the sample's spontaneous fluorescence[67]. Moreover, due to the nonlinear nature of two-photon absorption, its signal intensity is quadratically correlated with the excitation light intensity, allowing for the suppression of fluorescence away from the focal plane and thereby improving the spatial resolution of the imaging[68].

To obtain clear images, light with high power is commonly employed to excite the sample, which can lead to photobleaching or damage to the sample. To overcome this issue, the scheme of replacing classical light sources with entangled photon pairs was proposed[69]. Figure 7(a) shows the experimental setup of the entangled TPA microscope, where the entangled photon pairs are produced by the SPDC with a BBO crystal[34]. With a low excitation intensity of 3.6×10^7 photons/s of entangled two-photon pairs, which is a million times lower than the excitation level for the classical two-photon fluorescence image (1.5×10^{14} photon/s), images of breast cancer cells are captured, as shown in Fig. 7(b). This method enhances the two-photon absorption rate from a quadratic process to a linear one[70] and effectively reduces the required intensity of the excitation light. By using the entangled two-photon pair, a 10-order-of-magnitude reduction in excitation light power has been achieved in non-biological organic chemistry[71], and a 6-order-of-magnitude reduction has been obtained in breast cancer cells[34]. Moreover, the entangled two-photon pair has also been extended to other

atomic systems[72,73], molecules, and biological samples[74,75]. In addition to the entangled TPA fluorescence microscopy, entangled photon pairs have also been applied in the optical absorption microscope[76-78], where the SNR and precision of the transmittance estimation are improved.

5. Quantum-Enhanced Differential Interference Contrast Microscopy

The differential interference contrast microscopy (DIM) can transform the phase information into intensity information in the process of imaging[79,80]. Compared to classical phase contrast microscopy[81,82], it presents significant improvements in various aspects, such as resolution, contrast, and the thickness of samples that can be imaged[83]. Thus, it can be widely applied in living tissues or cells.

Figure 8(a) shows the experimental setup of DIM[38]. A polarizer transforms the input light into pure linearly polarized light. After passing through a Nomarski prism, the light splits into two spatially separated beams with perpendicular polarizations. By using a condenser lens, the two beams are focused onto the sample around 0.2 μm apart. Due to variations in thickness and refractive index of the sample, the two beams experience different phase shifts. After passing through the sample, the second lens, the Nomarski prism, and another polarizer, the interference signals of the two beams are collected by an intensity detector. When there is no phase shift difference between the two beams, the output signal remains constant. Otherwise, the intensity of the interference signal varies based on the sample structure. This enables DIM to present images resembling 3D relief, which indicates the distribution of the phase gradients of the sample.

Although DIM exhibits clear advantages in observing unstained samples, its imaging quality is still limited by the SNR when dealing with samples requiring low light conditions, such as photosensitive biological samples[84], quantum gases[85], and atomic ensembles[86]. In such scenarios, the use of non-classical light sources can help to improve the imaging quality. Figure 8(b) shows the experimental setup of the entanglement-enhanced DIM. By replacing the classical probe light with the NOON state, the SNR of the DIM is improved 1.35 times compared to the classical case, in the measurement of a glass plate carved with a Q-shaped relief[38]. The signals are mixed at a polarization beam splitter and then detected by a pair of single photon detectors. Figures 8(c) and 8(d) show the patterns of the sample observed using a single-photon source and two-photon NOON state, respectively, where the more distinct image is obtained in Fig. 8(d). Additionally, Figs. 8(e) and 8(f) show the further analysis of the images in the red region of Figs. 8(c) and 8(d), respectively, which reveals an improvement of the SNR from 1.58 ± 0.11 to 2.13 ± 0.12 when employing entangled photon sources.

In addition to DIM, the NOON state is also applied in super-sensitive polarization microscopy[87], where supersensitivity beyond the standard quantum limit is realized. By applying
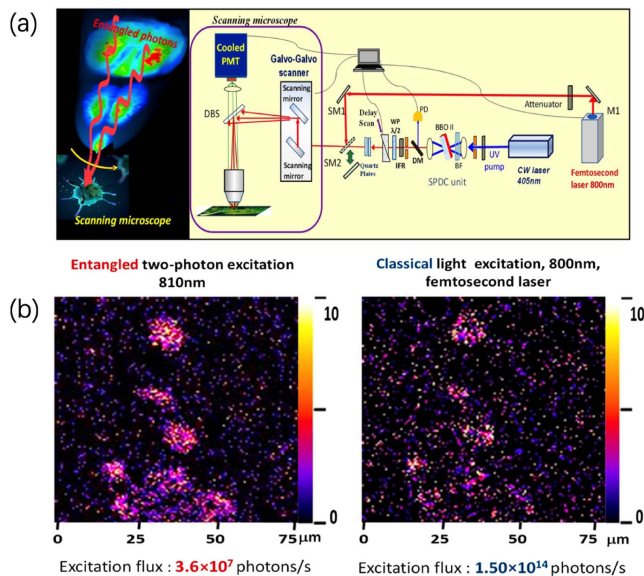

Fig. 7. (a) Experimental setup of the entangled TPA microscope[34]. (b) Images of breast cancer cells excited with the entangled two-photon (left) and the classical light (right), respectively.
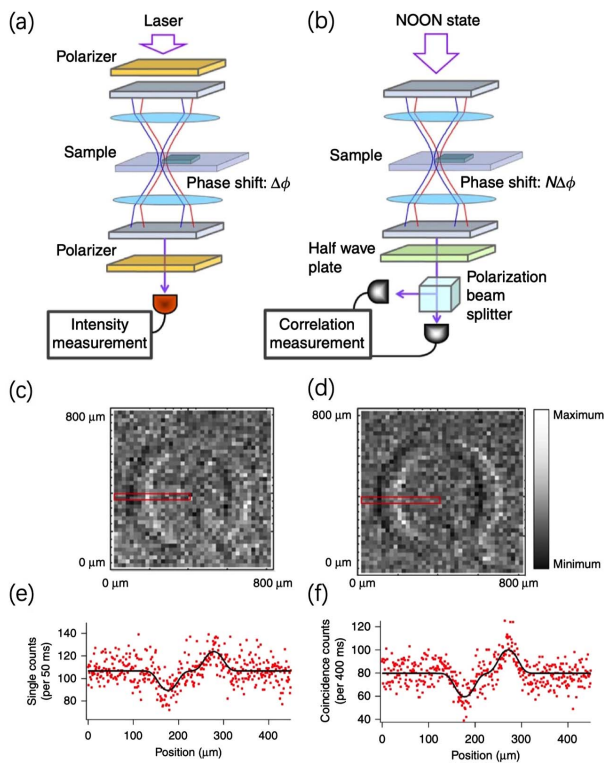
Fig. 8. Classical and quantum-enhanced DIM[38]. (a) Illustration of the classical DIM. (b) Illustration of the quantum-enhanced DIM. The red and blue lines represent different polarized light. (c) Image of the sample using a classical light. (d) Image of the sample using the two-photon entangled state. (e), (f) One-dimensional fine scan data for the area outlined in the red regions in (c) and (d) for the same photon number of 920.

entangled NOON states with $N = 2$ and $N = 3$ in the images of a sample of single quartz crystal, the improved phase images with sensitivity close to the Heisenberg limit are presented for a birefringent object. Furthermore, by increasing the photon number N of NOON state, the performance of microscopes will be further enhanced.

6. Conclusion

In this review, we briefly introduced squeezed light, entangled states, NOON state, and three types of quantum-enhanced microscopes based on different quantum states of light. Although the imaging mechanism of each microscope is different, they all show superior performance compared with conventional ones, which presents the advantages of quantum technologies. Quantum-enhanced SRS microscopy and DIM microscopy improve the SNR of imaging, and quantum-enhanced TPA microscopy reduces the required excitation power in imaging.

In quantum-enhanced SRS microscopy, the squeezed light is detected by an intensity photodetector or balanced homodyne detector after passing through a series of optical elements, including the object, sample, and condenser. The loss of these

optical elements leads to the decrease of the squeezing level of the squeezed light. Therefore, to maintain the squeezed noise of the squeezed light, it is essential to reduce the loss introduced by the employed optical elements and photodetector. In the entangled two-photon microscopy, it is essential to improve the input entangled photon flux, which may be useful to shorten the image collection time. In the quantum-enhanced DIM, the key challenge is to prepare NOON states with high photon numbers.

Recently, more quantum-enhanced microscopy techniques have also been developed, such as optical absorption microscopy[76-78], supersensitive polarization microscopy[87], and stimulated radiation microscopy[88]. With the development of quantum technology, these quantum-enhanced microscopic imaging techniques may become more and more practical and be applied in the fields of biology, medicine, and materials.

References

1. B. R. Masters, "History of the optical microscope in cell biology and medicine," in *Encyclopedia of Life Sciences* (2008).
2. A. Khodavirdipour, M. Mehregan, A. Rajabi, *et al.*, "Microscopy and its application in microbiology and medicine from light to quantum microscopy: a mini review," Avicenna J. Clin. Microbiol. Infect. **6**, 133 (2019).
3. R. E. Gordon, "Electron microscopy: a brief history and review of current clinical application," Methods Mol. Biol. **1180**, 119 (2014).
4. J. W. Lichtman and J. A. Conchello, "Fluorescence microscopy," Nat. Methods **2**, 910 (2005).
5. A. D. Elliott, "Confocal microscopy: principles and modern practices," Curr. Protoc. Cytom. **92**, e68 (2020).
6. H. J. Kimble, "The quantum internet," Nature **453**, 1023 (2008).
7. S. Wehner, D. Elkouss, and R. Hanson, "Quantum internet: a vision for the road ahead," Science **362**, 303 (2018).
8. A. Tavakoli, A. Pozas-Kerstjens, M. X. Luo, *et al.*, "Bell nonlocality in networks," Rep. Prog. Phys. **85**, 056001 (2022).
9. A. Pozas-Kerstjens, N. Gisin, and A. Tavakoli, "Full network nonlocality," Phys. Rev. Lett. **128**, 010403 (2022).
10. S. Pirandola, J. Eisert, C. Weedbrook, *et al.*, "Advances in quantum teleportation," Nat. Photonics **9**, 641 (2015).
11. P. Kok, W. J. Munro, K. Nemoto, *et al.*, "Linear optical quantum computing with photonic qubits," Rev. Mod. Phys. **79**, 135 (2007).
12. M. A. Nielsen and I. L. Chuang, *Quantum Computation and Quantum Information: 10th Anniversary Edition* (Cambridge University Press, 2011).
13. L. Gyongyosi and S. Imre, "A survey on quantum computing technology," Comput. Sci. Rev. **31**, 51 (2019).
14. M.-H. Wang, S.-H. Hao, Z.-Z. Qin, *et al.*, "Research advances in continuous-variable quantum computation and quantum error correction," Acta Phys. Sin. **71**, 060312 (2022).
15. V. Giovannetti, S. Lloyd, and L. Maccone, "Quantum-enhanced measurements: beating the standard quantum limit," Science **306**, 1330 (2004).
16. V. Giovannetti, S. Lloyd, and L. Maccone, "Advances in quantum metrology," Nat. Photonics **5**, 222 (2011).

17. C. Schäfermeier, M. Ježek, L. S. Madsen, *et al.*, "Deterministic phase measurements exhibiting super-sensitivity and super-resolution," Optica **5**, 60 (2018).

18. Z. Hou, R. J. Wang, J. F. Tang, *et al.*, "Control-enhanced sequential scheme for general quantum parameter estimation at the Heisenberg limit," Phys. Rev. Lett. **123**, 040501 (2019).

19. X. Zuo, Z. Yan, Y. Feng, *et al.*, "Quantum interferometer combining squeezing and parametric amplification," Phys. Rev. Lett. **124**, 173602 (2020).

20. M. Genovese, "Real applications of quantum imaging," J. Opt. **18**, 073002 (2016).

21. P.-A. Moreau, E. Toninelli, T. Gregory, *et al.*, "Imaging with quantum states of light," Nat. Rev. Phys. **1**, 367 (2019).

22. T. B. Pittman, Y. H. Shih, D. V. Strekalov, *et al.*, "Optical imaging by means of two-photon quantum entanglement," Phys. Rev. A **52**, R3429 (1995).

23. A. Gatti, E. Brambilla, M. Bache, *et al.*, "Correlated imaging, quantum and classical," Phys. Rev. A **70**, 013802 (2004).

24. A. Gatti, E. Brambilla, M. Bache, *et al.*, "Ghost imaging with thermal light: comparing entanglement and classical correlation," Phys. Rev. Lett. **93**, 093602 (2004).

25. A. Valencia, G. Scarcelli, M. D'Angelo, *et al.*, "Two-photon imaging with thermal light," Phys. Rev. Lett. **94**, 063601 (2005).

26. F. Ferri, D. Magatti, A. Gatti, *et al.*, "High-resolution ghost image and ghost diffraction experiments with thermal light," Phys. Rev. Lett. **94**, 183602 (2005).

27. J. H. Shapiro and R. W. Boyd, "The physics of ghost imaging," Quantum Inf. Process **11**, 949 (2012).

28. S. Lloyd, "Enhanced sensitivity of photodetection via quantum illumination," Science **321**, 1463 (2008).

29. S. H. Tan, B. I. Erkmen, V. Giovannetti, *et al.*, "Quantum illumination with Gaussian states," Phys. Rev. Lett. **101**, 253601 (2008).

30. E. D. Lopaeva, I. Ruo Berchera, I. P. Degiovanni, *et al.*, "Experimental realization of quantum illumination," Phys. Rev. Lett. **110**, 153603 (2013).

31. S. Barzanjeh, S. Guha, C. Weedbrook, *et al.*, "Microwave quantum illumination," Phys. Rev. Lett. **114**, 080503 (2015).

32. T. Gregory, P. A. Moreau, E. Toninelli, *et al.*, "Imaging through noise with quantum illumination," Sci. Adv. **6**, eaay2652 (2020).

33. J. H. Shapiro, "The quantum illumination story," IEEE Aerospace Electron. Syst. Mag. **35**, 8 (2020).

34. O. Varnavski, C. Gunthardt, A. Rehman, *et al.*, "Quantum light-enhanced two-photon imaging of breast cancer cells," J. Phys. Chem. Lett. **13**, 2772 (2022).

35. R. B. de Andrade, H. Kerdoncuff, K. Berg-Sørensen, *et al.*, "Quantum-enhanced continuous-wave stimulated Raman scattering spectroscopy," Optica **7**, 470 (2020).

36. C. A. Casacio, L. S. Madsen, A. Terrasson, *et al.*, "Quantum-enhanced nonlinear microscopy," Nature **594**, 201 (2021).

37. Z. Xu, K. Oguchi, Y. Taguchi, *et al.*, "Quantum-enhanced stimulated Raman scattering microscopy in a high-power regime," Opt. Lett. **47**, 5829 (2022).

38. T. Ono, R. Okamoto, and S. Takeuchi, "An entanglement-enhanced microscope," Nat. Commun. **4**, 2426 (2013).

39. A. I. Lvovsky, "Squeezed light," Photonics **1**, 121 (2015).

40. J.-C. Diels and W. Rudolph, "Fundamentals," in *Ultrashort Laser Pulse Phenomena*, Second Edition (Academic Press, 2006), p. 1.

41. Y. Eto, A. Koshio, A. Ohshiro, *et al.*, "Efficient homodyne measurement of picosecond squeezed pulses with pulse shaping technique," Opt. Lett. **36**, 4653 (2011).

42. Z. Qin, M. Wang, R. Ma, *et al.*, "Progress of the squeezed states of light and their application," Laser Optoelectron. Prog. **59**, 1100001 (2022).

43. H. Vahlbruch, M. Mehmet, K. Danzmann, *et al.*, "Detection of 15 dB squeezed states of light and their application for the absolute calibration of photoelectric quantum efficiency," Phys. Rev. Lett. **117**, 110801 (2016).

44. N. Corzo, A. M. Marino, K. M. Jones, *et al.*, "Multi-spatial-mode single-beam quadrature squeezed states of light from four-wave mixing in hot rubidium vapor," Opt. Express **19**, 21358 (2011).

45. S. Lorenz, C. Silberhorn, N. Korolkova, *et al.*, "Squeezed light from micro-structured fibres: towards free-space quantum cryptography," Appl. Phys. B **73**, 855 (2014).

46. A. Politi, M. J. Cryan, J. G. Rarity, *et al.*, "Silica-on-silicon waveguide quantum circuits," Science **320**, 646 (2008).

47. J. L. O'Brien, A. Furusawa, and J. Vučković, "Photonic quantum technologies," Nat. Photonics **3**, 687 (2009).

48. W. P. Bowen, R. Schnabel, P. K. Lam, *et al.*, "Experimental characterization of continuous-variable entanglement," Phys. Rev. A **69**, 012304 (2004).

49. C. Couteau, "Spontaneous parametric down-conversion," Contemp. Phys. **59**, 291 (2018).

50. C. K. Hong, Z. Y. Ou, and L. Mandel, "Measurement of subpicosecond time intervals between two photons by interference," Phys. Rev. Lett. **59**, 2044 (1987).

51. F. Bouchard, A. Sit, Y. Zhang, *et al.*, "Two-photon interference: the Hong-Ou-Mandel effect," Rep. Prog. Phys. **84**, 012402 (2021).

52. H. Paul, "Interference between independent photons," Rev. Mod. Phys. **58**, 209 (1986).

53. F. Shafiei, P. Srinivasan, and Z. Y. Ou, "Generation of three-photon entangled state by quantum interference between a coherent state and parametric down-conversion," Phys. Rev. A **70**, 043803 (2004).

54. H. F. Hofmann and T. Ono, "High-photon-number path entanglement in the interference of spontaneously down-converted photon pairs with coherent laser light," Phys. Rev. A **76**, 031806 (2007).

55. I. Afek, O. Ambar, and Y. Silberberg, "High-NOON states by mixing quantum and classical light," Science **328**, 879 (2010).

56. C. W. Freudiger, W. Min, B. G. Saar, *et al.*, "Label-free biomedical imaging with high sensitivity by stimulated Raman scattering microscopy," Science **322**, 1857 (2008).

57. M. Ji, S. Lewis, S. Camelo-Piragua, *et al.*, "Detection of human brain tumor infiltration with quantitative stimulated Raman scattering microscopy," Sci. Transl. Med. **7**, 309 (2015).

58. R. He, Y. Xu, L. Zhang, *et al.*, "Dual-phase stimulated Raman scattering microscopy for real-time two-color imaging," Optica **4**, 44 (2016).

59. W. J. Tipping, M. Lee, A. Serrels, *et al.*, "Imaging drug uptake by bio-orthogonal stimulated Raman scattering microscopy," Chem. Sci. **8**, 5606 (2017).

60. F. Hu, L. Shi, and W. Min, "Biological imaging of chemical bonds by stimulated Raman scattering microscopy," Nat. Methods **16**, 830 (2019).

61. Y. Li, B. Shen, S. Li, *et al.*, "Review of stimulated Raman scattering microscopy techniques and applications in the biosciences," Adv. Biol. **5**, e2000184 (2021).

62. K. M. Dean and A. E. Palmer, "Advances in fluorescence labeling strategies for dynamic cellular imaging," Nat. Chem. Biol. **10**, 512 (2014).

63. S. Oh, C. Lee, W. Yang, *et al.*, "Protein and lipid mass concentration measurement in tissues by stimulated Raman scattering microscopy," Proc. Natl. Acad. Sci. U.S.A. **119**, e2117938119 (2022).

64. J.-X. Cheng and X. S. Xie, *Coherent Raman Scattering Microscopy* (CRC Press, 2016).

65. M. J. B. Moester, F. Ariese, and J. F. de Boer, "Optimized signal-to-noise ratio with shot noise limited detection in stimulated Raman scattering microscopy," J. Eur. Opt. Soc. **10**, 15022 (2015).

66. Y. Ozeki, Y. Miyawaki, and Y. Taguchi, "Quantum-enhanced balanced detection for ultrasensitive transmission measurement," J. Opt. Soc. Am. B **37**, 3288 (2020).

67. P. T. C. So, C. Y. Dong, B. R. Masters, *et al.*, "Two-photon excitation fluorescence microscopy," Annu. Rev. Biomed. Eng. **2**, 399 (2000).

68. A. Ustione and D. W. Piston, "A simple introduction to multiphoton microscopy," J. Microsc. **243**, 221 (2011).

69. J. Gea-Banacloche, "Two-photon absorption of nonclassical light," Phys. Rev. Lett. **62**, 1603 (1989).

70. J. Javanainen and P. L. Gould, "Linear intensity dependence of a two-photon transition rate," Phys. Rev. A **41**, 5088 (1990).

71. D.-I. Lee and T. Goodson, "Entangled photon absorption in an organic porphyrin dendrimer," J. Phys. Chem. B **110**, 25582 (2006).

72. B. Dayan, A. Pe'er, A. A. Friesem, *et al.*, "Two photon absorption and coherent control with broadband down-converted light," Phys. Rev. Lett. **93**, 023005 (2004).

73. B. Dayan, A. Pe'er, A. A. Friesem, *et al.*, "Nonlinear interactions with an ultrahigh flux of broadband entangled photons," Phys. Rev. Lett. **94**, 043602 (2005).

74. O. Varnavski and T. Goodson, "Two-photon fluorescence microscopy at extremely low excitation intensity: the power of quantum correlations," J. Am. Chem. Soc. **142**, 12966 (2020).

75. J. P. Villabona-Monsalve, O. Varnavski, B. A. Palfey, *et al.*, "Two-photon excitation of flavins and flavoproteins with classical and quantum light," J. Am. Chem. Soc. **140**, 14562 (2018).

76. N. Samantaray, I. Ruo-Berchera, A. Meda, *et al.*, "Realization of the first sub-shot-noise wide field microscope," Light Sci. Appl. **6**, e17005 (2017).

77. M. Li, C.-L. Zou, D. Liu, *et al.*, "Enhanced absorption microscopy with correlated photon pairs," Phys. Rev. A **98**, 012121 (2018).

78. J. Sabines-Chesterking, A. R. McMillan, P. A. Moreau, *et al.*, "Twin-beam sub-shot-noise raster-scanning microscope," Opt. Express **27**, 30810 (2019).

79. G. Nomarski, "Microinterferometre differentiel a ondes polarisees," J. Phys. Rad. **16**, 9S (1955).

80. H. E. Rosenberger, "Differential interference contrast microscopy," in *Interpretive Techniques for Microstructural Analysis* (Springer US, 1977), p. 79.

81. F. Zernike and F. J. M. Stratton, "Diffraction theory of the knife-edge test and its improved form, the phase-contrast method," Mon. Not. R. Astron. Soc. **94**, 377 (1934).

82. C. R. Burch and J. P. P. Stock, "Phase-contrast microscopy," J. Sci. Instrum. **19**, 71 (1942).

83. X. Wang, H. Wang, J. Wang, *et al.*, "Single-shot isotropic differential interference contrast microscopy," Nat. Commun. **14**, 2063 (2023).

84. D. J. Stephens and V. J. Allan, "Light microscopy techniques for live cell imaging," Science **300**, 82 (2003).

85. K. Eckert, O. Romero-Isart, M. Rodriguez, *et al.*, "Quantum non-demolition detection of strongly correlated systems," Nat. Phys. **4**, 50 (2007).

86. F. Wolfgramm, C. Vitelli, F. A. Beduini, *et al.*, "Entanglement-enhanced probing of a delicate material system," Nat. Photonics **7**, 28 (2012).

87. Y. Israel, S. Rosen, and Y. Silberberg, "Supersensitive polarization microscopy using NOON states of light," Phys. Rev. Lett. **112**, 103604 (2014).

88. G. Triginer Garces, H. M. Chrzanowski, S. Daryanoosh, *et al.*, "Quantum-enhanced stimulated emission detection for label-free microscopy," Appl. Phys. Lett. **117**, 024002 (2020).